sustainability

MDPI

Article

Fuzzy Logic-Based LVRT Enhancement in Grid-Connected PV System for Sustainable Smart Grid Operation: A Unified Approach for DC-Link Voltage and Reactive Power Control

Mokabbera Billah [1], Shameem Ahmad [2], Chowdhury Akram Hossain [1], Md. Rifat Hazari [1], Minh Quan Duong [3], Gabriela Nicoleta Sava [4] and Emanuele Ogliari [5,*]

[1] Faculty of Engineering, American International University-Bangladesh, Dhaka 1229, Bangladesh; billahmokabbera@gmail.com (M.B.); chowdhury.akram@aiub.edu (C.A.H.); rifat@aiub.edu (M.R.H.)
[2] Department of Electrical and Electronic Engineering, BSRM School of Engineering, BRAC University, Dhaka 1212, Bangladesh; shameem.ahmad@bracu.ac.bd
[3] Electrical Engineering Faculty, The University of Da Nang—University of Science and Technology, Da Nang 550000, Vietnam; dmquan@dut.udn.vn
[4] Faculty of Power Engineering, National University of Science and Technology POLITEHNICA Bucharest, 060042 Bucharest, Romania; gabriela.sava@energ.pub.ro
[5] Department of Energy, Politecnico di Milano, Via Giuseppe La Masa, 34, 20156 Milan, Italy
* Correspondence: emanuelegiovanni.ogliari@polimi.it

Abstract

Low-voltage ride-through (LVRT) capability is essential for grid-connected photovoltaic (PV) systems, especially as rising renewable integration challenges grid stability during voltage disturbances. Existing LVRT methods often target isolated control functions, leading to limited system resilience. This paper presents a unified control strategy integrating DC-link voltage regulation, reactive power injection, and overvoltage mitigation using a coordinated fuzzy logic framework. The proposed architecture employs a cascaded control structure comprising an outer voltage loop and an inner current loop with feed-forward decoupling, synchronized via a Synchronous Reference Frame Phase-Locked Loop (SRF-PLL). At its core is a dual-input, single-output Fuzzy Logic Controller (FLC), featuring optimized membership functions and dynamic rule-based logic to manage multiple control objectives during grid faults. The proposed FLC-based unified LVRT controller for grid-tied PV system was implemented and validated for both symmetrical and asymmetrical fault conditions in MATLAB/Simulink 2023b platform. The proposed FLC-based LVRT controller achieves voltage sag compensation of 97.02% and 98.4% for symmetrical and asymmetrical faults, respectively, outperforming conventional PI control, which achieves 94.02% and 96.5%. The system maintains a stable DC-link voltage of 800 V and delivers up to 78% reactive power support during faults. Fault detection and recovery are completed within 200 ms, complying with Bangladesh grid code requirements. This integrated fuzzy logic approach offers a significant advancement for enhancing grid stability in high-renewable environments and supports reliable renewable utilization, and more sustainable grid operation in developing regions.

Keywords: LVRT; grid-tied PV system; fuzzy logic; DC-link voltage; reactive power injection; grid stability; smart grid; sustainable power grid

Academic Editor: Carlos Vargas-Salgado

Received: 12 January 2026
Revised: 12 February 2026
Accepted: 26 February 2026
Published: 3 March 2026

1. Introduction

The increasing integration of renewable energy sources, particularly photovoltaic (PV) systems, into the electrical grid has brought significant challenges for grid operators and utilities [1]. One of the critical challenges is ensuring the low-voltage ride-through (LVRT) capability of grid-connected PV systems during grid disturbances. These disturbances can lead to severe voltage fluctuations, causing PV inverters to trip and disconnect from the grid [1]. The sudden loss of power generation from PV systems can exacerbate the disturbance, potentially leading to cascading failures and compromising the stability and reliability of the entire power system.

To mitigate these issues, grid operators and regulatory bodies have established strict LVRT requirements, which mandate that grid-connected PV systems remain operational and provide reactive power support during grid disturbances [2]. These requirements are typically specified in grid codes or interconnection standards, which vary across different regions and countries. LVRT rules specify the voltage thresholds and timeframes during which PV systems are obligated to stay interconnected with the grid. As a reference, PV systems must stay functional even when the grid voltage decreases below 0% of the nominal value for a designated time, such as 150 ms [3]. Additionally, LVRT requirements often specify the reactive power injection profiles necessary to support voltage recovery during and after the disturbance event [4]. Furthermore, the widespread disconnection of PV systems during grid disturbances can exacerbate the disturbance and jeopardize the stability of the entire power system [5]. Therefore, developing effective control strategies to enhance the LVRT capability of grid-connected PV systems has become a crucial area of research.

Researchers have proposed several control strategies to improve the LVRT capability of grid-tied PV systems in line with grid codes. One method employs energy storage systems to retain power and support active/reactive power during faults [6], but it raises costs and may affect system reliability [7]. Another approach uses a two-stage converter to manage reactive and active currents [8], yet it fails to fully mitigate AC overvoltage and DC-link overvoltage. A strategy targeting positive and negative sequences focuses only on asymmetrical faults and lacks effective DC-link regulation and active power injection during faults [9]. To control DC-link overvoltage, hardware-based methods like DC-breaking choppers [10], energy storage units [11], and series dynamic braking resistors [12] have been proposed. Although effective, these solutions involve high costs and frequent maintenance, limiting their practicality for widespread use.

Researchers have investigated control strategies that modify MPPT algorithms or operate in non-MPPT modes during faults, such as power-weakening control [13], fault current limiting [14], and non-MPPT fuzzy logic control [15]. These often focus on steady-state performance and lack comprehensive evaluation under varying irradiance and fault types. In [16], a discrete-time LVRT controller with resonant compensators mitigates DC-link oscillations and harmonics under asymmetrical faults but does not address symmetrical faults. A modified SOGI-PLL scheme in [17] improves zero-voltage ride-through for single-phase PV systems but may cause amplitude overshoot. To overcome linear controller limitations, Fuzzy Logic Controllers (FLCs) have been proposed for LVRT due to their ability to manage nonlinearities [18]. An FLC using instantaneous power theory improves response during voltage sags [19], though it lacks focus on the full dynamic range from fault onset to clearance and optimal reactive power injection [20]. Intelligent MPPT methods like RBFN-based [21] and GRNN-PSO-based controllers [22] show adaptability but are complex and costly, limiting practical deployment.

Recent control strategy advancements have furthered LVRT research. Joshi et al. [23] proposed a strategy combining active power curtailment (APC) with prioritized reactive

power injection for voltage recovery at the PCC, meeting grid code requirements. However, it focuses only on unbalanced voltage sags and involves complex parameter tuning, such as pseudo inverter capacity (PIC). Zhang et al. proposed an event-triggered distributed hybrid control scheme that achieves accurate power sharing without relying on detailed network parameters, restores key operating parameters (e.g., frequency), and reduces communication cost via event-triggered update protocols [24].

Saxena et al. [25] developed a Modified Dual SOGI-based Model Predictive Control (MDSOGI-MPC) for multifunctional PV systems, enabling dynamic power estimation and LVRT operation. Despite its effectiveness, the high computational load limits implementation on low-cost microcontrollers, and its two-stage three-phase setup reduces broader applicability. Elmi and Yildirim [26] introduced a chaotic nonlinear MPC (CNMPC) for OPV systems to improve MPPT efficiency and manage power during faults, but its computational complexity and untested relevance to silicon-based PV systems present concerns. Gira and Dahiya [27] proposed an ANFIS-based control scheme for rooftop PV systems, enabling active and reactive power supply through converter optimization, yet its high computational demand limits real-time use in low-cost systems. Current LVRT research often focuses on isolated objectives like reactive power injection [13], current limiting [14], or DC-link voltage stabilization [15], lacking a unified control strategy that integrates all goals. Many methods rely on fixed parameters or predefined rules [19], limiting adaptability under varied fault conditions. Recent LVRT research has shown that combining virtual inductance with DC-link voltage boosting can substantially strengthen converter fault performance by suppressing transient overcurrent and improving voltage support capability [28]. Though some approaches excel in individual functions—like voltage support [13]—they may neglect other aspects, such as DC-link stability. This highlights the need for a comprehensive control solution capable of optimizing multiple objectives simultaneously. Most research still relies on conventional PI controllers, while advanced methods like model predictive, intelligent, and adaptive control remain underutilized. Table 1 compares key LVRT techniques and features.

Table 1. Aspects of different LVRT techniques.

Authors	Control Strategy	Contribution	Limitations
[6]	Two-stage conversion	Active, reactive power are supported by storing power.	Increased costs. Impacts power system reliability.
[8]	Positive, negative sequence control	Regulates reactive, active current.	Overlooks DC-link voltage increase.
[9]	Hardware-based solutions	Suitable for large-scale PV plants.	Does not sort DC-link overvoltage.
[10–12]	Modified MPPT algorithms	Address DC-link overvoltage efficiently.	It is limited to asymmetrical faults.
[13–15]	Discrete-time LVRT controller	Power-weakening control.	Primarily focus on steady-state performance.
[16]	Modified SOGI-PLL scheme	Non-MPPT fuzzy logic control.	Additional hardware costs.
[17]	Fuzzy Logic Controllers (FLCs)	DC-link voltage oscillations mitigation.	Requires frequent maintenance.
[19]	RBFN and GRNN-based MPPT	Zero-voltage ride-through control.	Does not address optimal reactive power injection.

Table 1. *Cont.*

Authors	Control Strategy	Contribution	Limitations
[21,22]	Two-stage conversion using Instantaneous power theory.	Handles nonlinearities and uncertainties.	Steady-state performance. Lack of proper evaluations.
[23]	Current limitation	Improved current control	Focused on only the unbalanced condition.
[25]	MPC with Modified Dual SOGI.	Enhanced power quality, PCC voltage assist.	Limited to two-stage three-phase systems.
[26]	Chaotic-based Nonlinear Model Predictive Control.	Improved LVRT; better dynamic response during grid faults.	Limited to organic PV; not tested with silicon-based PV.
[27]	Adaptive Neuro-Fuzzy Inference System.	STATCOM for reactive power compensation.	Computationally intensive; limited to small-scale PV.

Although existing FLC-based LVRT strategies effectively regulate active and reactive power during grid disturbances, a gap remains in integrating FLC-based inverter control with robust DC-link voltage regulation. DC-link voltage is vital in grid-tied PV systems, as its stability impacts inverter performance and reliability. Grid disturbances can cause power imbalance between the PV array and the grid, resulting in DC-link voltage fluctuations that may lead to inverter tripping, damage, or inefficiency. Therefore, a unified LVRT strategy is needed—one that harnesses FLC's strength in managing nonlinearities and uncertainties to regulate both active/reactive power and maintain DC-link voltage within safe, efficient limits during disturbances.

This work proposes an inclusive unified LVRT control strategy for a single-stage three-phase PV power plant connected to the Bangladeshi grid, where DC-link protection, overvoltage mitigation, and grid code reactive support are coordinated under one supervisory framework. In contrast to many earlier LVRT approaches that address DC-link stabilization and reactive current injection as separate or sequential functions, the proposed strategy integrates these objectives to improve ride-through capability and post-fault recovery while maintaining inverter–grid connection. The main contributions are:

- Unified integrated control architecture for LVRT: A coordinated control framework is developed that jointly manages DC-link voltage regulation, reactive current support, and mode switching during voltage sags, enabling consistent operation and ride-through compliance under representative fault scenarios.
- Fuzzy-logic-assisted multi-objective mitigation and smooth transition: A fuzzy logic decision layer is introduced to adapt control actions during disturbances, mitigating DC-link overvoltage caused by power imbalance during symmetrical and asymmetrical faults and ensuring smooth transition between normal and LVRT operation. This reduces abrupt switching effects and improves robustness under nonlinear transient dynamics compared with fixed-gain or purely PI-based approaches.
- Grid-support enhancement with quantitative LVRT evaluation: Grid-code-aligned reactive power injection is incorporated to accelerate voltage recovery and enhance grid stability. The effectiveness of the unified strategy is validated via simulation using clear quantitative indicators as voltage compensation and DC-link Overshoot and comparative analysis against baseline control cases for both symmetrical and asymmetrical faults.

The remainder of this paper is organized as follows: Section 2 presents the grid code requirements and the system modeling and control methodology, including the proposed FLC-based unified LVRT strategy. Section 3 describes the simulation setup and discusses the results under representative grid disturbances, including comparative

analysis against baseline controllers in terms of voltage recovery, reactive power support, and LVRT compliance. Section 4 presents the conclusion, key findings, contributions, and future research directions.

2. Materials and Methods

2.1. Grid Requirement

The Bangladesh Grid Code 2019, section 5.9, under the title requirements for VRE generators, specifies LVRT requirements for Variable Renewable Energy (VRE) genera-tors, including grid-connected PV systems [29]. It mandates that VRE Generating Plants must remain connected during voltage dips based on a defined voltage-time profile. As in Figure 1, key parameters include: staying connected for at least 0.15 s if voltage drops to zero in any phase; maintaining connection for 0.60 s if voltage remains above 30% of nominal in all phases; and remaining connected indefinitely if voltage stays at or above 90% of nominal in all phases [29].

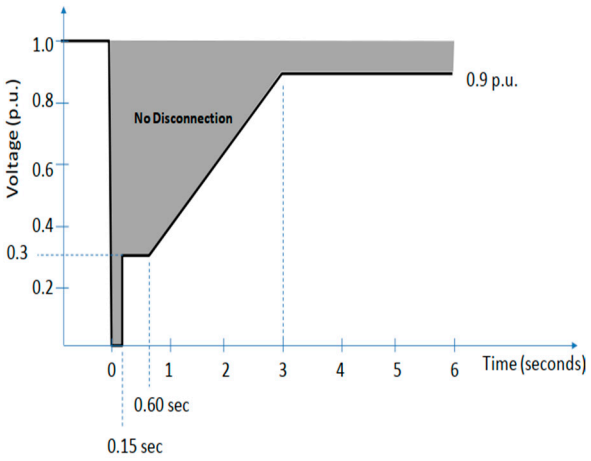

Figure 1. LVRT requirements [29].

In the proposed controller, the fault is detected, and the inverter transitions to LVRT mode within approximately 200 ms (0.2 s), which falls within the 0.15 s and 0.60 s ride-through boundary interval of the LVRT voltage–time profile in Figure 1, thereby satisfying the grid code timing requirement for maintaining connection and initiating grid support.

2.2. PV Module Equivalent Circuit and PV Array Sizing

The most commonly adopted model for PV is the single-diode equivalent circuit, which balances simplicity with sufficient accuracy for most applications [30,31]. A mathematical model establishes the correlation between a PV module's output voltage and current, while also providing a method to determine the photocurrent generated under specific environmental conditions [32,33]. This work modeled a grid-tied PVPP with a capacity of 1.5 MWp using MATLAB/Simulink, as detailed in Table 2.

$$I_L = I_{PH} - I_{sat}\left(e^{\frac{qV_d}{mNS^{KT}}} - 1\right) - \frac{I_L R_s + V_L}{R_p} \quad (1)$$

$$I_{PH} = [I_{sc} + \alpha_i\left(T - T_{ref}\right)]\frac{G}{G_{ref}} \quad (2)$$

$$I_{sc} = I_{sc,ref}\left(\frac{R_p + R_s}{R_p}\right) \quad (3)$$

$$I_{sat} = \frac{\left[I_{sc.ref} + \alpha_i\left(T - T_{ref}\right)\right]}{\left(e^{q\left(\frac{V_{oc,raf}\alpha_v(T-T_{ref})}{mN_sKT}\right)}\right) - 1} \quad (4)$$

where I_L = PV output current, I_{ph} = photocurrent, I_{sat} = diode reverse saturation current, V_L = PV output voltage, m = diode ideality factor, K = Boltzmann's constant, R_s = series resistance, and R_p = shunt resistance.

Table 2. Properties of PV modules.

Features of the PV Module	Value
Maximum-power-current	I_{mp} = 8.04 A
Maximum-power-voltage	V_{mp} = 49.78 V
Maximum-power	P_{max} = 400 W
Short-circuit-current	I_{sc} = 8.56 A
Open-circuit-voltage	V_{oc} = 60 V
Temperature coefficient of I_{sc}	$\alpha_i = 0.043/°C$
Temperature coefficient of V_{oc}	$\alpha_v = -0.367/°C$
Parallel and series resistance (R_p, R_s)	389.9 Ω, 0.33 Ω
Maximum-power	P_{max} = 400 W

The P-V and I-V properties of PV modules are confirmed using simulations conducted under typical test settings, with irradiance temperature, T_{ref} = 25 °C, and G_{ref} = 1000 W/m^2, and the parameters of the equivalent circuit and Equations (1)–(4) are listed in Table 2, as provided by the manufacturers in the datasheet (TOPSUN solar modules). The array configuration is optimized to balance voltage and current requirements for grid integration. The array consists of 235 parallel strings, 16 modules connected in series [19,33], giving maximum power point current (I_{mpv}) of 1889.4 A and a maximum power point voltage (V_{mpv}) of 796.4 V, power of 1,504,718.1 W under standard test conditions.

2.3. Modeling of Grid-Tied PV

The grid-tied photovoltaic system consists of several key components that convert solar energy into grid-compatible electricity. The PV array generates DC power from sunlight, then processed through power electronic converters and filters before grid injection. Figure 2 shows the schematic of a grid-connected PV.

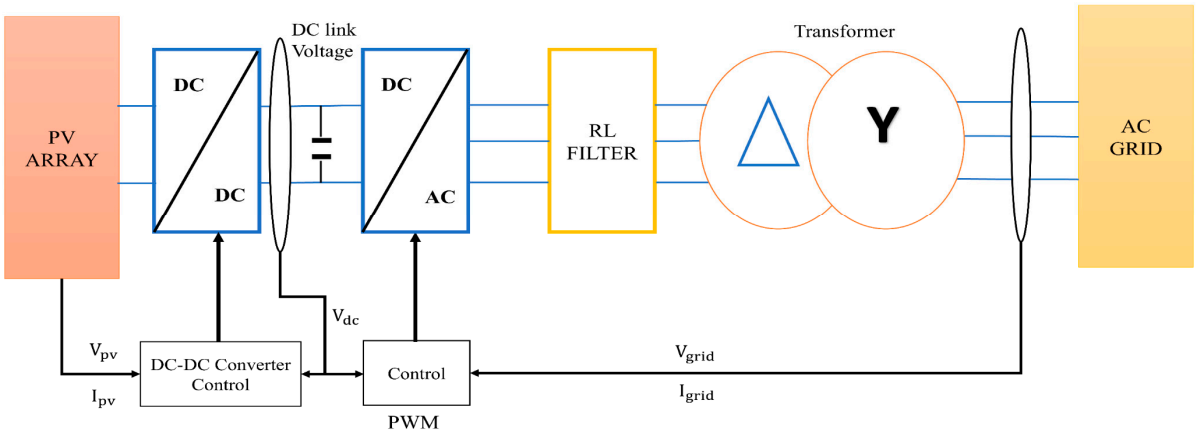

Figure 2. Illustration of a grid-tied PV system.

In this paper, unified strategy refers to a coordinated LVRT control architecture that simultaneously addresses (i) DC-link overvoltage mitigation (boost duty PI loop), (ii) grid code reactive current support (I_q reference law), and (iii) dynamic current/power reference shaping via FLC, all triggered by a common sag detection and mode switching logic.

The first stage uses a DC-DC converter, controlled via a dedicated controller that monitors the PV array's voltage (V_{pv}) and current (I_{pv}) [30]. In Boost converter design, continuous conduction mode is assumed, where duty cycle D denotes the switch ON time and D′ the OFF time. The governing equations are as follows:

$$\frac{dI_L}{dt} = \frac{1}{L}[V_{in}D + (V_{in} - V_0)D'] \quad (5)$$

$$\frac{dV_0}{dt} = \frac{1}{C}(I_L D' - \frac{V_0}{R}) \quad (6)$$

where C is the boost capacitance, R is the equivalent load seen at the converter output, V_0 is the converter output voltage, and I_L is the inductor current. Moreover, the correlation between the duty cycle D and the voltage is expressed as:

$$V_0 = \frac{V_{in}}{1 - D} \quad (7)$$

The inverter, typically employing Pulse Width Modulation (PWM) techniques, converts the DC power to AC power compatible with the grid frequency. A control system governs the inverter operation, taking feedback from the grid voltage (V_{grid}) and current (I_{grid}) to ensure proper synchronization and power quality [32]. The inverter side voltage, current, and power supplied are denoted as:

$$V_{ac}(t) = \sqrt{2}V_{rms}(sin\,\omega t) \quad (8)$$

$$I_{ac}(t) = \sqrt{2}I_{rms}(sin\,\omega t) \quad (9)$$

$$P_{ac}(t) = V_{ac}(t).\, I_{ac}(t) = V_{rms}I_{rms}[1 - cos\,(2\omega t)] \quad (10)$$

Following the inverter, an RL filter helps to smooth out high-frequency components in the output waveform, reducing harmonics and improving power quality [34]. The filtered AC power then passes through a transformer [35]: it steps up the voltage to match the grid level and isolates the PV system from the grid. The parameters utilized in the proposed system are detailed in Table 3.

Table 3. Specifications of the suggested framework [19].

Specification	Values
DC-link Voltage (V_{dc})	800 V
Grid Voltage (V_{grid})	33 kV
Transformer	0.4/33 kv
DC-link Capacitor (C_{dc})	0.2130 F
Grid frequency, ω	$2\pi \times 50$ rad/s
R filter of the inverter, R	1.25 Ω
L filter of the inverter, L	0.1 mH
PI Parameter of Voltage Loop	K_p = 1.2, K_i = 50
PI Parameter of Current Loop	K_p = 0.4, K_i = 8

2.4. DC-Link Voltage Control

While traditional MPPT techniques, such as perturb and observe and incremental conductance, perform well under varying environmental conditions, they are limited

during grid faults due to significant DC-link voltage fluctuations, which impair power injection efficiency [33,36]. To address this, in Figure 3, a control strategy inspired by [37] has been integrated into the power conversion stage, employing a PI controller that regulates the DC-link voltage without MPPT algorithms. The threshold of 1.05 pu is selected to provide a practical protection margin above the nominal DC-link voltage while avoiding unnecessary activation due to normal ripple and measurement noise.

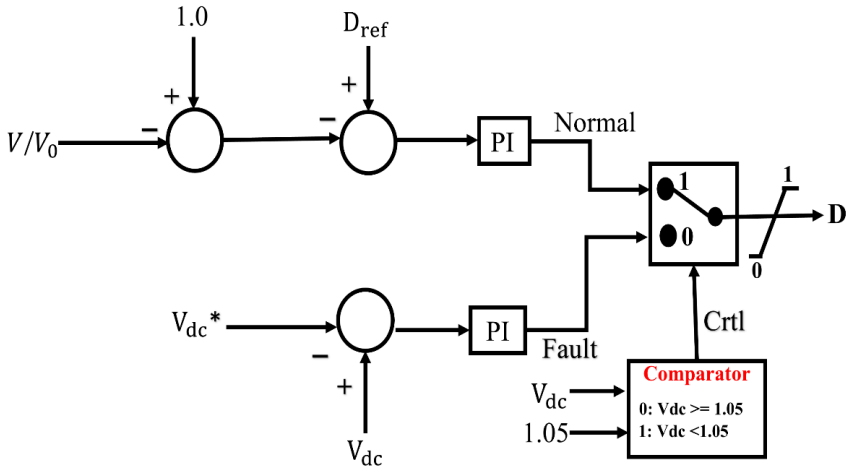

Figure 3. Proposed DC-DC converter control.

The controller activates when the DC-link voltage exceeds 1.05 pu, maintaining it within safe limits during both normal and fault conditions to enhance system stability [37]. The governing law is defined by:

$$\boldsymbol{u(t)} = K_p * \boldsymbol{e(t)} + K_i * \int e(t)dt \quad (11)$$

where u(t) = control signal (duty cycle for the boost converter), e(t) = error signal, K_p = proportional gain, K_i = integral gain.

The control's primary functions are to sustain the DC-link voltage at its nominal level, regulate power flow from the PV array to the grid inverter, and enhance system stability during grid disturbances. The control system continuously monitors the DC-link voltage (V_{dc}) and compares it to a reference value (V_{dc_ref}).

When (V_{dc}) exceeds a threshold of 1.05 per unit, the control algorithm activates to regulate the voltage. The control algorithm involves measuring the actual DC-link voltage, calculating the error $e(t) = V_{dc\_ref} - V_{dc}$, and computing the control signal u(t) using the Proportional-Integral (PI) control law, where K_p is 1, and K_i is 0.01, which are taken by tuning the PI controller using the pidtune command.

2.5. Inverter Control Strategy

The grid-connected inverter system utilizes an advanced control mechanism to ensure efficient power transfer from the PV array to the utility grid, as illustrated in Figure 4. This control mechanism maintains the DC-link voltage at its nominal level, which is critical for the reliable operation of the inverter. The system features a cascaded structure, comprising an outer voltage control loop and an inner current control loop [38].

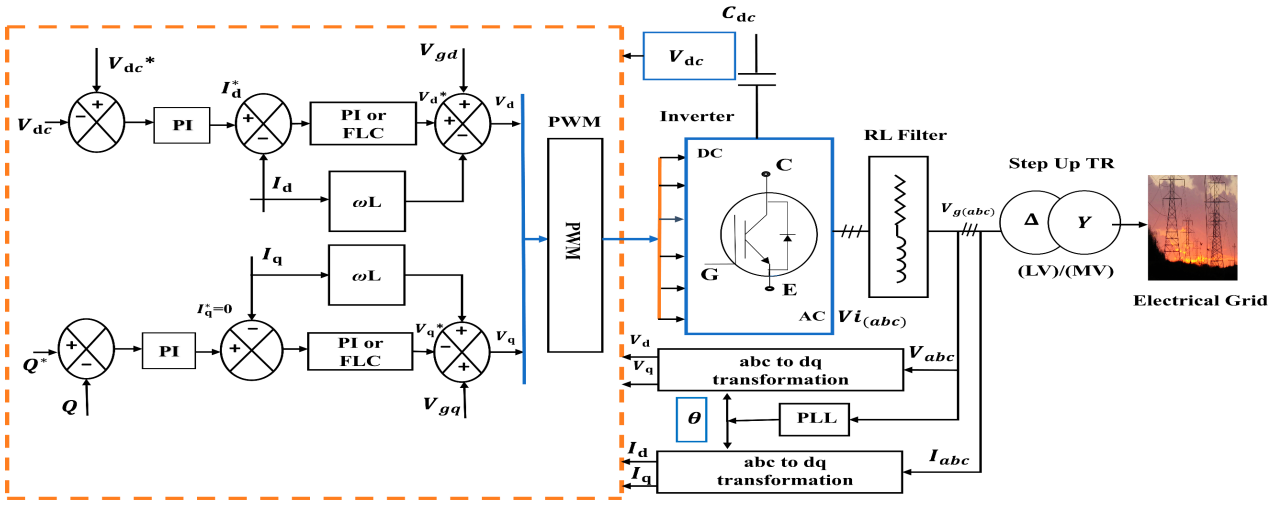

Figure 4. Schematic of grid inverter control [33].

The outer loop uses a PI controller to compare the reference DC-link voltage (V_{dc}) with the measured value. The output of this controller generates the reference for the active current component (I_d), which is used by the inner current control loop [31,32]. Under normal operating conditions, which is 0.9 pu to 1.1 pu [34], the control strategy aims to inject the maximum active power into the grid while minimizing reactive power generation [33]. In the synchronous reference frame (d-q), the inner current control loop calculates the voltage references (V_d) and (V_q) based on the current references (I_d) and (I_q) [39]. These d-q frame voltages are then converted into three-phase (abc) reference frame voltages [39]. The resulting three-phase voltage references are fed into the PWM generator, which produces the switching signals for the inverter [40,41]. The system employs Sinusoidal Pulse Width Modulation (SPWM). The mathematical representation of the grid-tied inverter in the abc frame is as follows:

$$\begin{aligned} V_{ia} &= \boldsymbol{L}\frac{di_a}{dt} + Ri_a + V_{ga} \\ V_{ib} &= \boldsymbol{L}\frac{di_b}{dt} + Ri_b + V_{gb} \\ V_{ic} &= \boldsymbol{L}\frac{di_c}{dt} + Ri_c + V_{gc} \end{aligned} \tag{12}$$

where V_{ia}, V_{ib}, V_{ic} represent the inverter output voltages, grid voltages are presented by V_{ga}, V_{gb}, V_{gc}, and i_a, i_b, i_c represent the inverter output currents. By applying a rotational synchronous d-q reference frame transformation, the inverter output voltages can be transformed dq0 components:

$$V_{id} = \boldsymbol{L}\frac{di_d}{dt} + Ri_d + V_{gd} V_{iq} = \boldsymbol{L}\frac{di_q}{dt} + Ri_q + V_{gq} \tag{13}$$

Active and reactive power injected into the grid can be calculated in the d-q frame as

$$\boldsymbol{P} = \frac{3}{2}\left(V_{gd} I_d + V_{qd} I_q\right) \tag{14}$$

$$\boldsymbol{Q} = \frac{3}{2}\left(-V_{gd} I_d + V_{qd} I_q\right) \tag{15}$$

Assuming a balanced system with negligible grid power losses, the power equations

$$\boldsymbol{P} = \frac{3}{2} V_{gd} I_d \tag{16}$$

$$\boldsymbol{Q} = -\frac{3}{2} V_{gd} I_q \tag{17}$$

During grid fault conditions, as shown in Figure 5, the inverter must rapidly transition into LVRT mode to maintain grid stability. The proposed control mechanism employs a fault detection algorithm that continuously monitors the grid voltage. When a fault is detected, the controller seamlessly switches to LVRT mode. This mode activates a specialized control algorithm designed to manage the system's response to the fault condition. The fault detection equation is

$$V_g = \sqrt{V_d^2 + V_q^2} \tag{18}$$

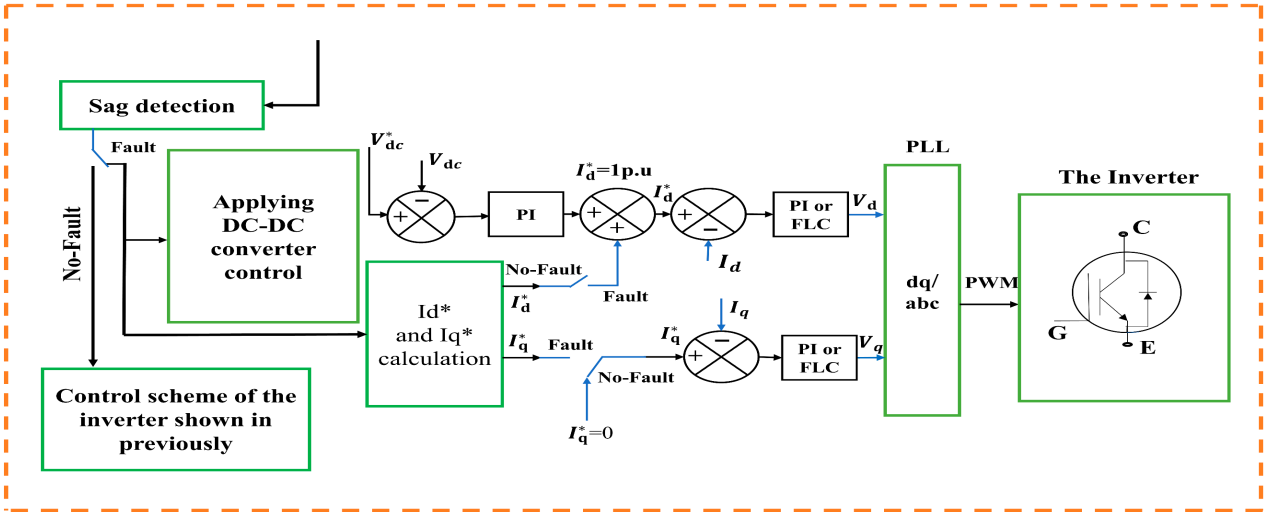

Figure 5. Schematic of unified LVRT control.

This control strategy is characterized by its capability to dynamically modify reactive power injection in response to the intensity of the voltage sag. The adaptive approach is essential for maintaining grid voltage during LVRT operation. Upon detection of a voltage sag, the control system calculates the required reactive current injection according to the following relationship:

$$\begin{aligned} \boldsymbol{I_q} &= 0; \quad V_{gp} \geq 0.9\boldsymbol{V_{gn}} \\ I_q &= -2\tfrac{V}{Vgn} + 2; \quad 0.9V_{gn} \geq V_{gp} > 0.5V_{gn} \\ \boldsymbol{I_q} &= 1; \quad V_{gp} \leq 0.5\boldsymbol{V_{gn}} \end{aligned} \tag{19}$$

V_{gp} and V_{gn} denote the magnitude of the voltage present during a fault and the normal grid voltage, respectively.

2.6. FLC Architecture and Structure

This study implements a Fuzzy Logic Controller (FLC) for grid-tied inverters, offering a robust alternative to conventional controllers that rely on precise system modeling. Utilizing fuzzy set theory, linguistic variables, and IF-THEN rules, the FLC provides adaptive control for nonlinear systems with inherent uncertainties [42]. The proposed dual-input, single-output FLC structure, illustrated in Figure 6, accepts the error signals $\Delta I_d(t)$, $\Delta I_q(t)$, and their rates of change ($\frac{d}{dt}\Delta I_d(t)$, $\frac{d}{dt}\Delta I_q(t)$) as input generating a control action u(t). This configuration outperforms single- and triple-input alternatives in both dynamic response and steady-state accuracy. To enhance low-voltage ride-through (LVRT), the FLC coordinates Reactive Power Injection and Active Power Management during faults. It operates in three stages:

- Fuzzification: Converts crisp inputs into fuzzy values.
- Inference: Applies rule-based logic.

- Defuzzification: Translates fuzzy outputs into crisp control actions via the Center of Gravity (COG) method.

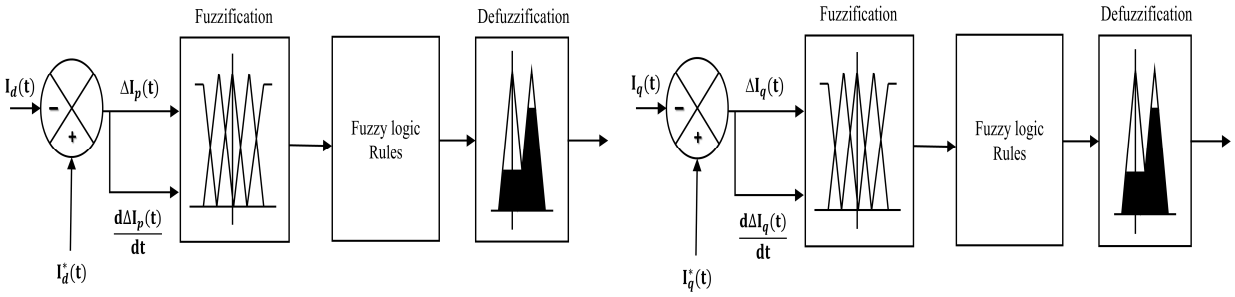

(**a**) (**b**)

Figure 6. Suggested fuzzy controller: voltage reference extraction (**a**) active power, and (**b**) reactive power [19].

Triangular membership functions, selected for simplicity and computational efficiency [19], are defined for each input using five linguistic terms: Negative Large (NL), Negative Small (NS), Zero (ZE), Positive Small (PS), and Positive Large (PL), as shown in Figure 7. Five linguistic terms are used for the inputs (error and change-of-error) to capture finer operating conditions around the equilibrium and during fast transients. In contrast, three output sets (ZE/ME/LA) are used to keep the controller computationally light and to limit the aggressiveness of the control action, which improves robustness during switching-level implementation. Increasing output granularity (e.g., five output MFs) would increase tuning effort and could lead to higher sensitivity to noise without a proportional improvement in LVRT performance. The membership function for a triangular fuzzy set is mathematically expressed as

$$\mu_A(x) = \begin{cases} 0, & x \le a, \\ \frac{x-a}{b-a}, & a < x \le b \\ \frac{c-x}{c-b}, & b < x \le c \\ 0, & x > c \end{cases} \tag{20}$$

where x is the crisp input (error or rate of change in error), and a, b, and c are the parameters defining the triangular membership function for a specific fuzzy set.

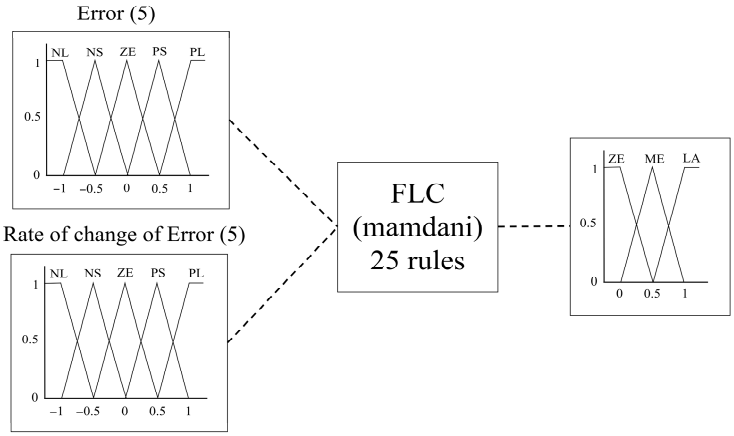

Figure 7. Input and output ranges for fuzzy logic.

The input range is normalized to [−1, +1] to ensure robustness and scalability. For the output (control action), three triangular membership functions—Zero (ZE), Medium (ME), and Large (LA)—are defined over the interval [0, +1]. This three-level granularity balances control resolution and computational efficiency. Fuzzy inference maps the input fuzzy sets to the output using a predefined rule base. The Mamdani inference method is adopted for its intuitive rule construction and smooth output transitions [42]. Each rule follows the standard IF–THEN format:

$$R_{ij}: \textbf{\textit{IF}}\ \Delta I_d(t)\ \textbf{\textit{is}}\ A_i\ \textbf{\textit{AND}}\ \frac{d}{dt}\Delta I_d(t)\ \textbf{\textit{is}}\ B_j\ \textbf{\textit{THEN}}\ \boldsymbol{\mu}(t)\ \textbf{\textit{is}}\ C_k, \tag{21}$$

where A_i and B_j are fuzzy sets for the input variables, C_k is the fuzzy set for the output variable, $\mu(t)$ is the control action. The firing strength of each rule is computed using the min operator (for AND operations):

$$a_{ij} = \min(\mu_{Ai}(\Delta I_d(t)),\ \mu_{Bj}\left(\frac{d}{dt}\Delta I_d(t)\right)) \tag{22}$$

The output fuzzy set for each rule is then computed as

$$\mu_{ck}(\boldsymbol{u}) = \min\left(a_{ij}, \mu_{Ck}(u)\right) \tag{23}$$

The overall output fuzzy set is obtained by aggregating the outputs of all rules using the max operator:

$$\mu_{output}(\boldsymbol{u}) = \max(\mu_{C1}(u), \mu_{C2}(u), \ldots, \mu_{c25}(\boldsymbol{u})) \tag{24}$$

The defuzzification process converts the fuzzy output into a crisp control signal. The Center of Gravity (COG) method is employed for its ability to provide smoother control actions and better steady-state accuracy compared to alternatives like the mean of maximum (MOM) [35]. The crisp control action u(t) is computed as

$$\boldsymbol{u}(t) = \frac{\int_0^1 u\ .\ \mu_{output}(u)\ du}{\int_0^1 \mu_{output}(u)\ du} \tag{25}$$

This structured approach ensures the FLC is finely tuned for optimal operation in grid-connected systems, with the rule base, central to the FLC, developed as a 5 × 5 matrix to control actions, as shown in Table 4, following a systematic methodology that included initial rule formulation based on control engineering principles and grid-connected inverter behavior, physical interpretation to ensure each rule has a clear physical meaning, consistency verification to avoid conflicting control actions, and completeness analysis to cover all possible input combinations.

Table 4. Fuzzy control rules.

Rate of Change in Error	Error				
	NL	**NS**	**ZE**	**PS**	**PL**
NL	LA	LA	LA	LA	LA
NS	LA	LA	LA	LA	ME
ZE	LA	LA	LA	ME	ZE
PS	LA	LA	ME	ZE	ZE
PL	LA	ME	ZE	ZE	ZE

Each rule is formulated based on control engineering principles and the behavior of grid-connected inverters. For example, when the error is NL and its rate is NL, the controller outputs LA to produce a strong corrective action and quickly restore the controlled variable. Conversely, when error and rate are PL, the output is ZE to avoid overcorrection and reduce oscillations.

The rule base ensures consistency, completeness, and physical interpretability [41], as validated through simulations under normal operation, symmetrical faults, and asymmetrical faults. The integration of this FLC in the grid-connected inverter control system improves its capacity to sustain stable operation under fluctuating grid circumstances [41] and effectively regulate power flow [43].

3. Results and Discussions

The effectiveness of the chosen approach to control for grid-tied PV systems is evaluated using the MATLAB/Simulink 2023b platform. The inverter is operated using sinusoidal PWM (SPWM) as described in Section 2.5. To ensure result reproducibility and consistent controller timing, a discrete switching simulation is adopted using a fixed-step formulation. The simulation settings were fixed-step discrete solver, simulation step, T_{sim} = 5 µs, controller sampling time, T_c = 100 µs, and PWM switching frequency, f_{sw} = 5 kHz. The grid at the PCC is modeled in Simscape Electrical as a Thevenin source using a Three-Phase Source on the 33-kV side. The grid strength is represented by setting SCR = 10 and X/R = 10. Faults are applied at the PCC using the Simscape Electrical "Three-Phase Fault" block with initial status = 0, switching times = ([4 5]) s, fault resistance R_{on} = 0.001 Ω. The performance was tested for both symmetrical (L-L-L) and asymmetrical (L-L) faults. For the L-L case, the faulted phases are A-B, while for the L-L-L case the faulted phases are A-B-C using the same timing and resistance settings. For asymmetrical faults, only line-to-line fault results presented because the results for line-to-ground and line-to-line faults were almost the same. To assess the practicality of the suggested strategy, a fault was created at 4 s and was cleared after 1 s. To ensure consistent interpretation across all cases, the following indices are used. And for both symmetrical and asymmetrical faults, voltage compensation is computed with respect to the nominal (pre-fault) PCC voltage magnitude, using the RMS magnitude. For the DC-link Overshoot and faults:

$$OS_{Vdc}(\%) = \frac{V_{dc,peak} - V_{dc,nom}}{V_{dc,nom}} \times 100 \tag{26}$$

$$\text{Compensation}(\%) = \frac{V_{PCC,fault}^{RMS}}{V_{PCC,pre}^{RMS}} \times 100 \tag{27}$$

where $V_{dc,nom}$ = reference DC voltage, $V_{dc,peak}$ = maximum observed DC-link voltage during the fault interval, $V_{PCC,pre}^{RMS}$ = steady-state pre-fault RMS voltage at the PCC, and $V_{PCC,fault}^{RMS}$ = RMS voltage during the fault when the LVRT controller is active.

The execution of the DC-link voltage control has shown significant efficacy in preserving DC-link voltage stability under fault scenarios. Without this control, DC-link voltage spikes reached up to 2500 V during faults, as shown in Figure 8a, and with the control, the DC-link voltage remained within 800 V even under fault conditions, as shown in Figure 8b. This stability not only protects system components but also ensures continuous power delivery to the grid. Also, the PV side voltage and power stay stable, as shown in Figure 9a,b. Figure 9c,d show the output based on Figure 1, where the run time is 6 s, and the fault occurs in 0.15 s. These outputs show little to no

differences from Figure 9a,b, and the voltage and power go back to the nominal value within 0.60 s.

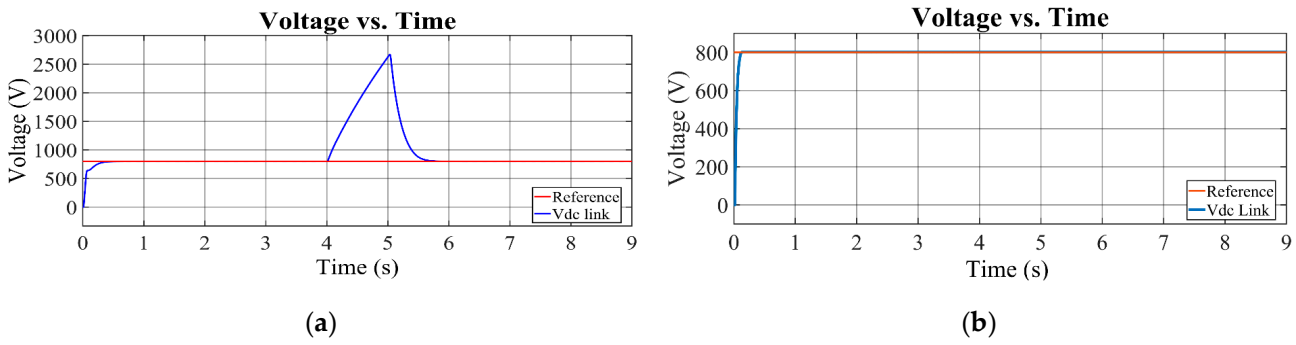

(**a**) (**b**)

Figure 8. DC-link voltage (**a**) without and (**b**) with DC-link control.

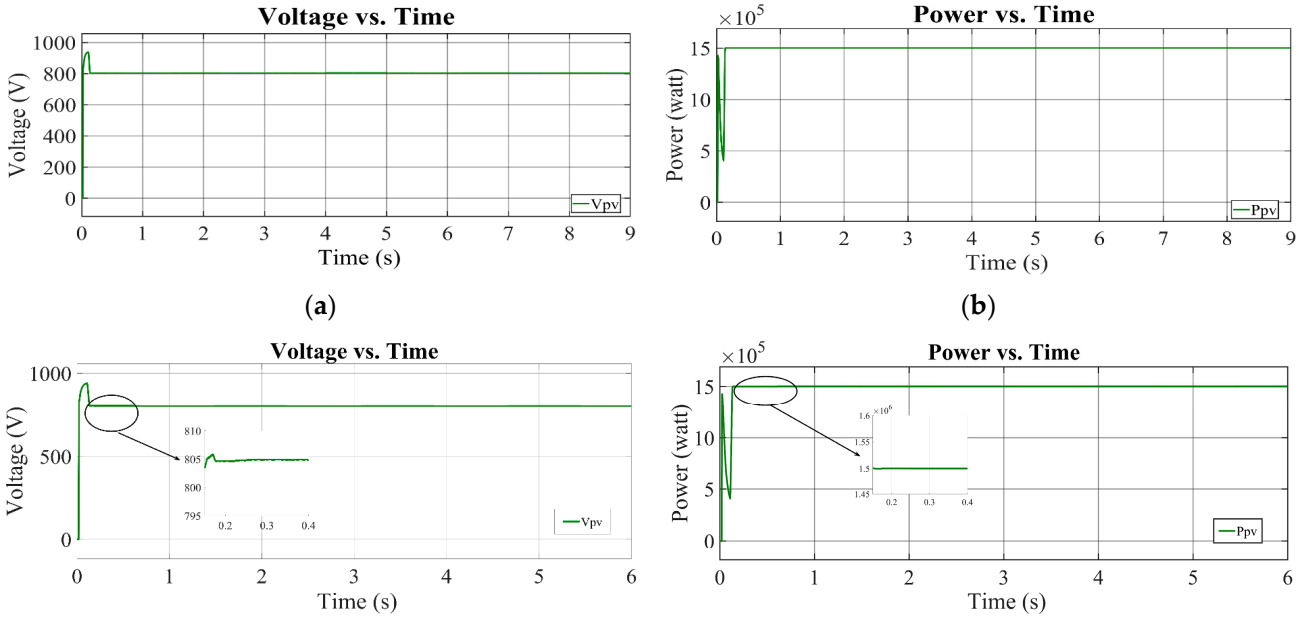

(**a**) (**b**)

(**c**) (**d**)

Figure 9. During fault (**a**) PV voltage (0–9 s), (**b**) PV power (0–9 s), (**c**) PV voltage (0–6 s), and (**d**) PV power (0–6 s).

3.1. Symmetrical Fault Analysis

For a symmetrical fault, Figure 10a,b show the grid voltage with no LVRT control. Figure 10c,d show voltage is compensated by 94.02% using the proposed control with PI. For FLC, Figure 10e,f show that the sag is compensated to 97.02%. The inverter voltage that goes almost zero during fault without LVRT control, as shown in Figure 11a, is compensated 95.703% while using PI-based LVRT control and 96.8% for using FLC-based LVRT control in Figure 11c,e.

The active and reactive power consumption during a symmetrical fault for both PI and FLC are illustrated in Figure 12a–d. Real power drops to almost 0%. During a fault, reactive power is injected 97% for PI and 85% for FLC; after the fault is cleared, it becomes minimal.

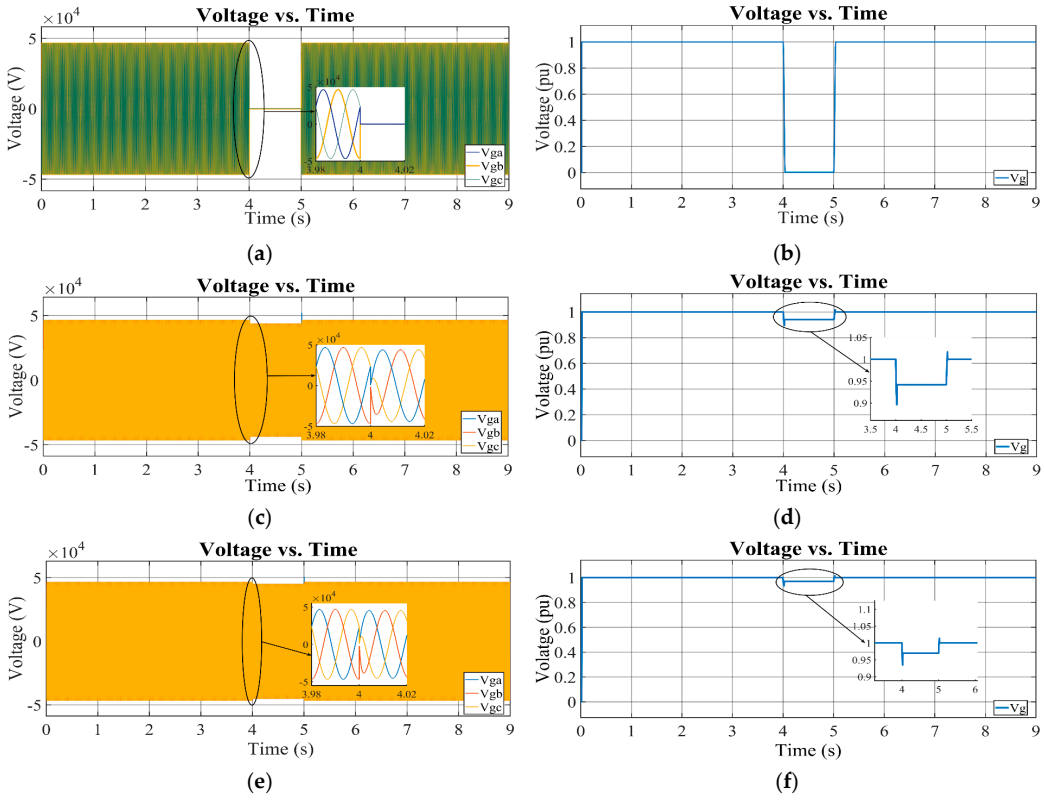

Figure 10. Grid voltages during L-L-L fault: without LVRT (**a**) sinusoidal, (**b**) RMS; PI (**c**) sinusoidal, (**d**) RMS; FLC (**e**) sinusoidal, and (**f**) RMS.

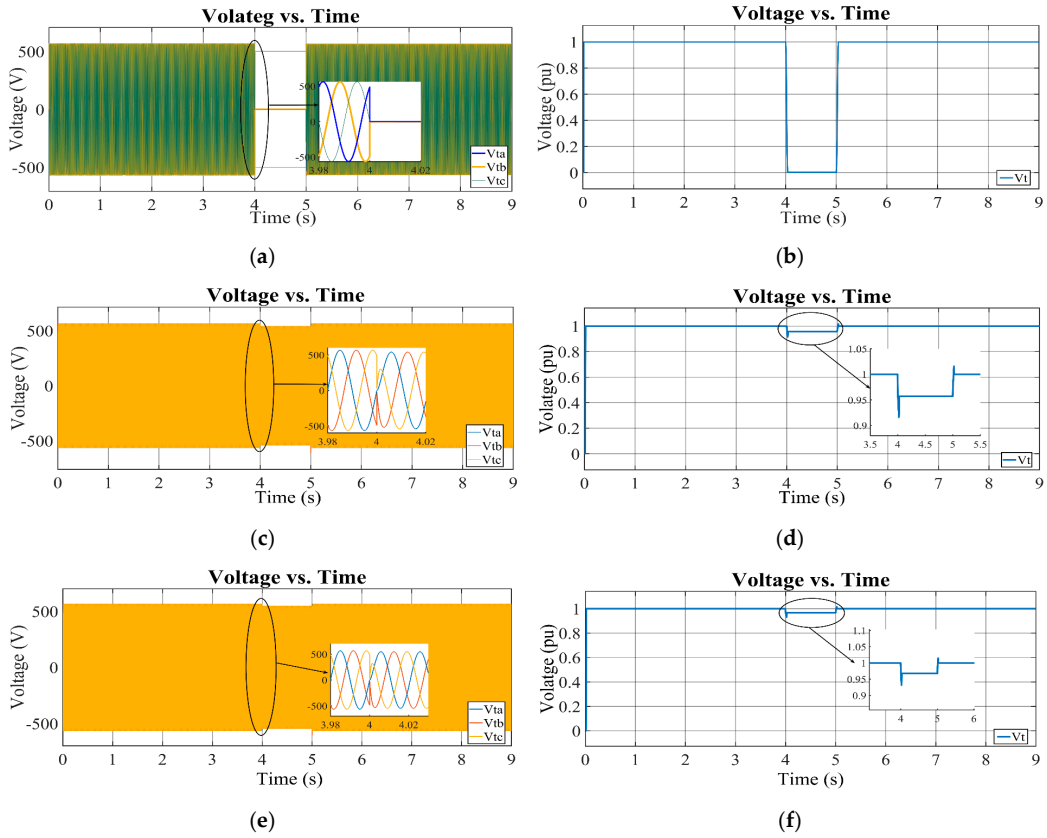

Figure 11. Inverter voltages during L-L-L fault: without LVRT control (**a**) sinusoidal, (**b**) RMS; PI (**c**) sinusoidal, (**d**) RMS; FLC (**e**) sinusoidal, and (**f**) RMS.

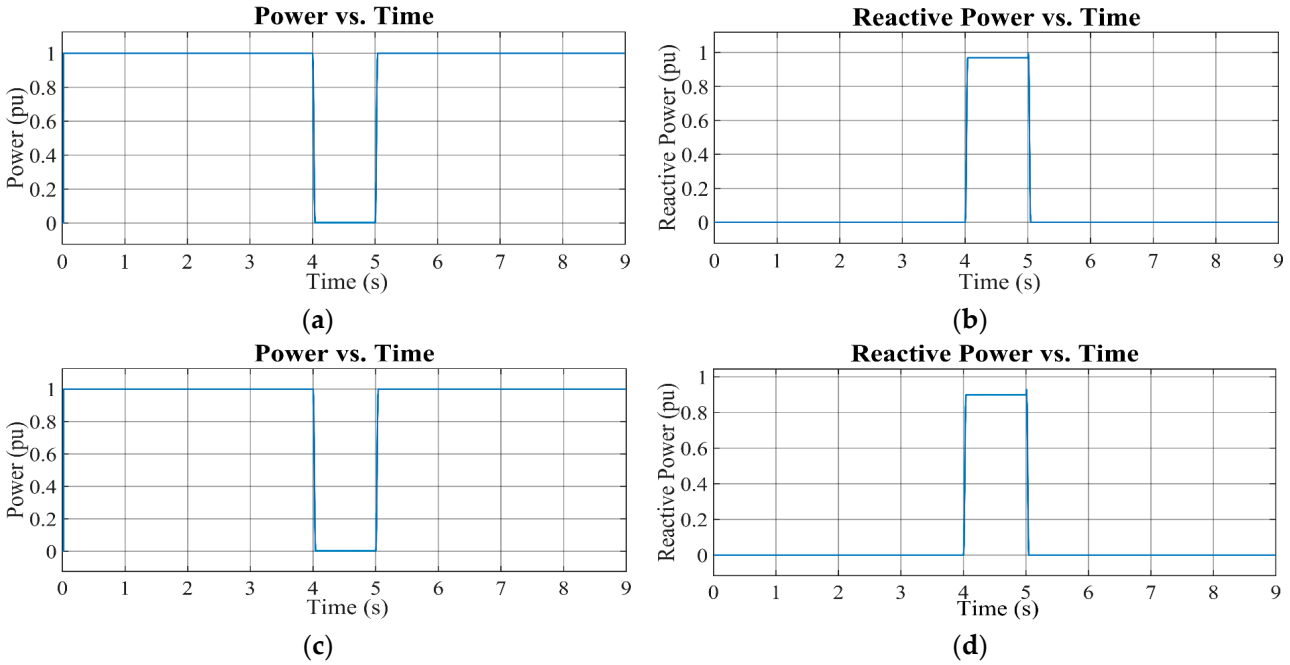

Figure 12. During L-L-L fault with LVRT, PI (**a**) real power, and (**b**) reactive power; FLC (**c**) real power, and (**d**) reactive power.

3.2. Asymmetrical Fault Analysis

As depicted in Figures 13a,b and 14a,b during an asymmetrical (L-L) fault, the grid and inverter voltages drop to approximately 45% when using conventional control methods. The grid and inverter voltages are shown in Figures 13c,d and 14c,d during asymmetrical fault while using the proposed strategy with PI. The grid voltage is compensated at 96.5%, and the inverter voltage is compensated at 96.23%. For FLC, Figures 13e,f and 14e,f show that grid voltage sag is compensated up to 98.4% and the inverter voltage is compensated up to 97.98%.

Figure 15 illustrates the usage of actual power and reactive power. During a fault, actual power consumption decreases by 90% for PI and 63% for fuzzy and subsequently rises to its prior form after fault clearing, whereas reactive power consumption increases by 78% for PI and 67% for fuzzy during the fault and then decreases to a minimum post-clearance.

PI and FLC implementations provide enough active and reactive power supply to improve grid voltage stabilization. While FLC-based control compensates for the sag better, the dynamic response for PI-based control is slightly better than fuzzy. For symmetrical and asymmetrical faults, PI-based control takes 200 ms for both cases, but fuzzy takes a bit longer to respond during the L-L fault.

Both control methods effectively complied with the Bangladesh Grid Code specifications for voltage restoration and reactive power delivery. This enhanced stability contributes to the reliability of individual PV installations and the overall robustness of the Bangladeshi power grid.

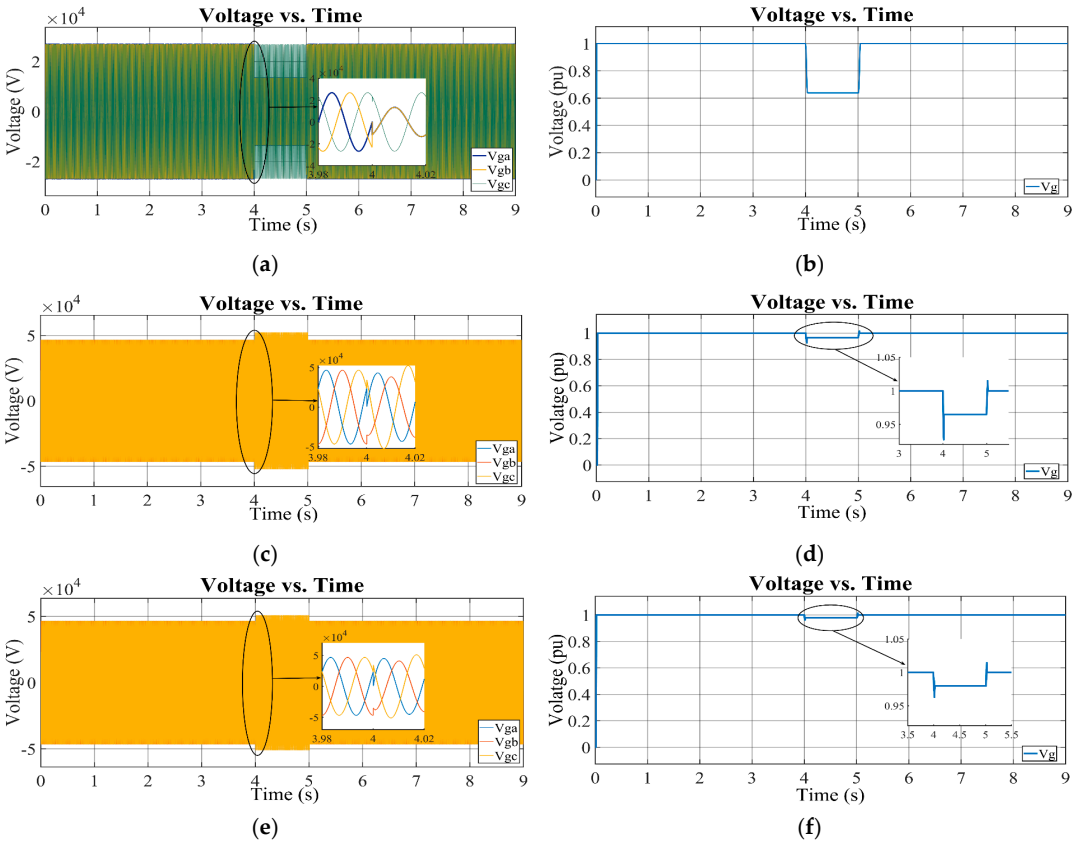

Figure 13. Grid voltages during L-L fault: without LVRT (**a**) sinusoidal, (**b**) RMS; PI (**c**) sinusoidal, (**d**) RMS; FLC (**e**) sinusoidal, and (**f**) RMS.

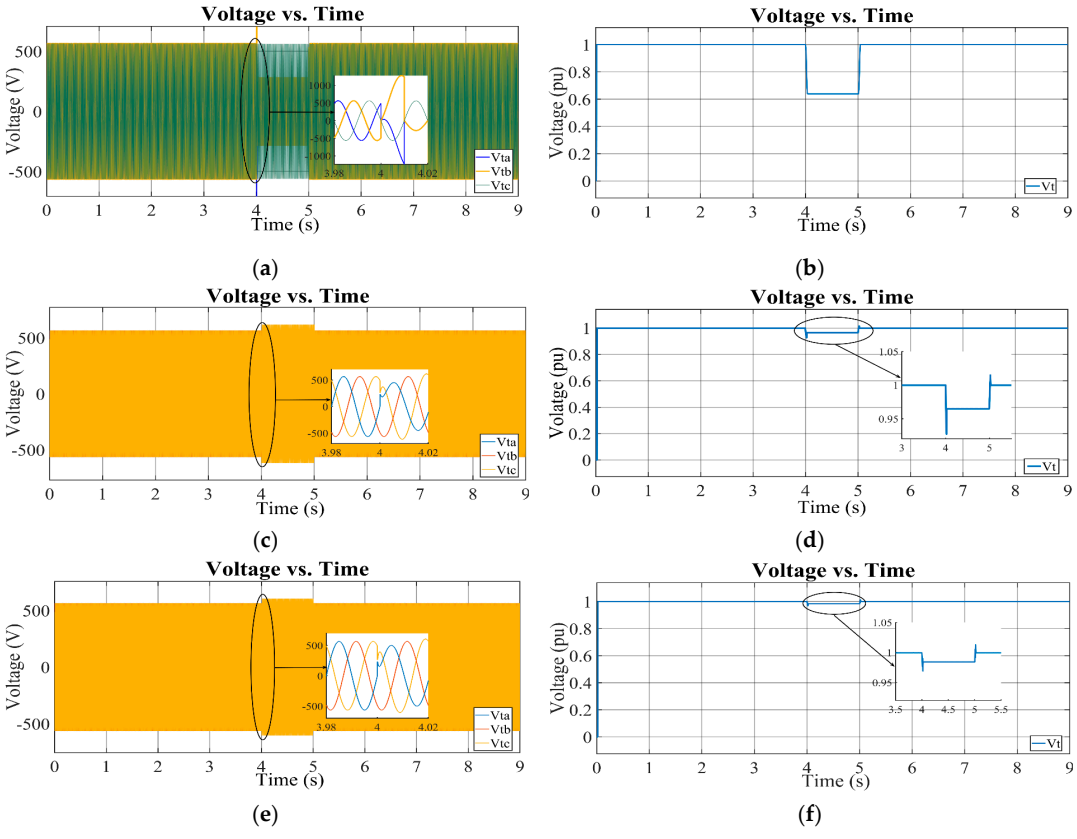

Figure 14. Inverter voltages during L-L fault: without LVRT (**a**) sinusoidal, (**b**) RMS; PI (**c**) sinusoidal, (**d**) RMS; FLC (**e**) sinusoidal, (**f**) RMS.

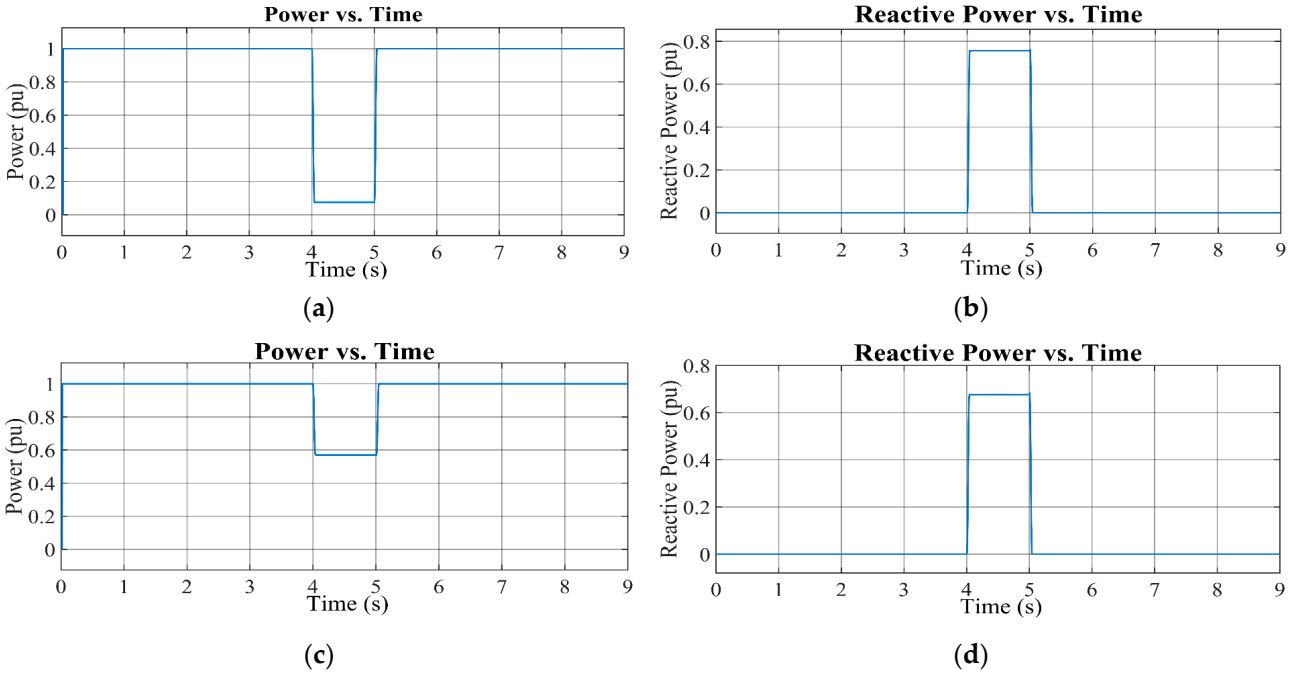

Figure 15. During L-L fault with LVRT, PI (**a**) real power, and (**b**) reactive power; FLC (**c**) real power, and (**d**) reactive power.

3.3. Comparative Analysis

Table 5 compares control methods where the values are taken from the authors' original scenario for managing symmetrical and asymmetrical faults in grid-connected PV systems, assessing DC-link voltage stability, Grid/Inverter Voltage Recovery, reactive power injection, and voltage sag. Traditional controllers, PI+STFCL and PI+BFCL [14], show limited effectiveness. PI+STFCL struggles with oscillations, achieving only 10% and 25% Grid Voltage Recovery in symmetrical and asymmetrical faults. PI+BFCL improves recovery to 62.5% (symmetrical) and 87% (asymmetrical), but spikes and sag persist. SD+BFCL [14] performs slightly better. The PI+DC chopper [33] shows 15% and 92% recovery with oscillations. FLC [43] enhances performance, though some spikes occur during fault clearance. To move beyond qualitative curve inspection, the LVRT performance is also evaluated using the quantitative indicators reported in Table 5, compensation, and DC Overshoot (%) computed from the indices defined in this section. For the symmetrical fault, the proposed PI controller achieves 94.02% Grid Voltage Recovery and 95.703% Inverter Voltage Recovery with 0.25% DC Overshoot, while the proposed fuzzy controller improves the recovery to 97.01% (Grid) and 96.8% (Inverter) with the same 0.25% DC Overshoot. For the asymmetrical (L–L) fault, the proposed PI controller reaches 96.5% Grid Voltage Recovery and 96.23% Inverter Voltage Recovery with 0.125% DC Overshoot, whereas the proposed fuzzy controller achieves 98.4% (Grid) and 97.98% (Inverter) with 0.125% DC Overshoot. These numerical results confirm that the proposed unified strategy improves voltage-recovery performance while maintaining very small DC-link stress, consistent with the transient waveforms and the LVRT timing requirement discussed in the same section.

Table 5. Comparison between proposed and existing LVRT controllers.

Methods \ Aspects	Fault Type	DC-Link Voltage	Grid Voltage Recovery	Inverter Voltage Recovery	Reactive Power Injection	Voltage Sag W/o Control	DC Overshoot with Controller
PI+STFCL [14]	Symmetrical	Wide oscillation with many spikes	0%	Not mentioned	Not mentioned	~90% sag	Not mentioned
	Asymmetrical (L-G)	Wide oscillation	25%	Not mentioned	Not mentioned	~90% sag	Not mentioned
PI+BFCL [14]	Symmetrical	Oscillation with small spikes	62.5% with spikes	Not mentioned	Not mentioned	~90% sag	Not mentioned
	Asymmetrical (L-G)	Post-fault small oscillations	90% with spikes	Not mentioned	Not mentioned	~87% sag	Not mentioned
SD+BFCL [14]	Symmetrical	Pre-fault spikes	62.5%	Not mentioned	Not mentioned	~90% sag	Not mentioned
	Asymmetrical (L-G)	Pre-fault small oscillations	94% with spikes	Not mentioned	Not mentioned	~85% sag	Not mentioned
PI+DC chopper [33]	Symmetrical	Pre-fault and post-fault oscillation	15%	Not mentioned	A small amount is injected	Not mentioned	Not mentioned
	Asymmetrical (L-L)	Oscillation during pre-fault and post-fault	92%	Not mentioned	A small amount is injected	Not mentioned	Not mentioned
FLC-based control [43]	Symmetrical	Significant voltage increases during a fault	~88%	Not mentioned	I_q is injected during the fault	~100% sag	Not mentioned
	Asymmetrical (L-L)	Spikes during fault clearance	~90%	Not mentioned	I_q is injected during fault	~95% sag	Not mentioned
Proposed Control with PI	Symmetrical	Negligible oscillation	94.02%	95.703%	A sufficient amount is injected	~100% sag	~0.25%
	Asymmetrical (L-L)	Negligible oscillation during pre- or post-fault	96.5%	96.23%	A sufficient amount is injected	~45% sag	~0.125%
Proposed Control with Fuzzy	Symmetrical	Negligible oscillation	97.01%	96.8%	A sufficient amount is injected	~100% sag	~0.25%
	Asymmetrical (L-L)	Negligible oscillation	98.4%	97.98%	A sufficient amount is injected	~45% sag	~0.125%

4. Conclusions

This study proposes a robust control strategy for grid-tied PV systems that complies with the Bangladesh Grid Code and enhances LVRT performance. The method combines DC-link voltage regulation, overvoltage suppression, and reactive power injection. Both PI

and FLC met code requirements; FLC offered superior voltage sag compensation, though with a slower response to asymmetrical faults. Simulation results confirmed stable grid operation and voltage recovery during disturbances. For symmetrical faults, voltage compensation reached 94.02% with PI and 97.02% with FLC; under asymmetrical faults, the rates were 96.5% and 98.4%, respectively. These findings support improved reliability and scalability for large-scale PV integration in Bangladesh. The approach offers a practical model for developing countries aiming to expand renewable energy while ensuring grid stability.

Future work will extend the validation to include detailed power-quality assessment like THD of inverter and grid currents in pre-fault, fault, and post-fault intervals, and a systematic sensitivity analysis under varying grid strength, line impedance, and operating conditions. In addition, the proposed unified LVRT strategy will be validated using hardware-in-the-loop (HIL) to confirm real-time performance and implementation robustness.

Author Contributions: Conceptualization, E.O., S.A. and M.B.; Methodology, M.B., S.A. and E.O.; Software, M.B. and S.A.; Validation, S.A., C.A.H., M.R.H., M.Q.D., G.N.S. and E.O.; Investigation, S.A., M.R.H., M.B. and C.A.H.; Writing—original draft, M.B. and S.A.; Writing—review & editing, S.A., C.A.H., M.R.H., M.Q.D., G.N.S., M.B. and E.O.; Visualization, M.B., M.R.H., M.Q.D. and G.N.S. All authors have read and agreed to the published version of the manuscript.

Funding: This research received no external funding.

Institutional Review Board Statement: Not applicable.

Informed Consent Statement: Not applicable.

Data Availability Statement: The data used for this research are contained within the article.

Conflicts of Interest: The authors declare no conflict of interest.

References

1. Ahmad, S.; Mubarak, H.; Jhuma, U.K.; Ahmed, T.; Mekhilef, S.; Mokhlis, H. Point of Common Coupling Voltage Modulated Direct Power Control of Grid-Tied Photovoltaic Inverter for AC Microgrid Application. *Int. Trans. Electr. Energy Syst.* **2023**, *2023*, 3641907. [CrossRef]
2. Rumky, T.T.J.; Ahmed, T.; Ahmed, M.; Ahmad, S.; Rahman, M.M. Performance of microgrid systems on multiple dynamic loads penetration. In Proceedings of the IEEE International Conference on Power Systems, Cox's Bazar, Bangladesh, 13–15 December 2023; pp. 1–6.
3. Tenaga, S. *Grid Code for Peninsular Malaysia*; Energy Commission Malaysia: Putrajaya, Malaysia, 2023; Rep. GC-2023.
4. Hossain, Z.; Ahmad, S.; Jhuma, U.K.; Mekhilef, S.; Mubin, M.; Mokhlis, H.; Ahmed, T. A Flexible Interconnection and Power Sharing Strategy for Two Autonomous Microgrid Systems. In Proceedings of the IEEE 6th International Conference on Computing, Communication and Automation (ICCCA), Arad, Romania, 17–19 December 2021; pp. 472–477.
5. Jhuma, U.K.; Mekhilef, S.; Ahmad, S.; Islam, J.; Jesan, J.R.; Billah, M.M. The Impact of Synchronous Generator on Voltage Sag Mitigation in Power System Network. In Proceedings of the IEEE 4th International Conference on Computing, Power and Communication Technologies (GUCON), Kuala Lumpur, Malaysia, 24–26 September 2021; pp. 1–5.
6. Kordkheili, S.F.H.; Hamzeh, M. AC Fault Ride-Through Strategy for MMC-Based HVDC Systems with Short Lines. In Proceedings of the Power Electronics, Drive Systems, and Technologies Conference (PEDSTC), Babol, Iran, 31 January–2 February 2023; pp. 1–6.
7. Worku, M.Y.; Abido, M.A. Grid-connected PV array with supercapacitor energy storage system for fault ride through. In Proceedings of the IEEE International Conference on Industrial Technology (ICIT), Seville, Spain, 17–19 March 2015; pp. 2901–2906.
8. Nithya, C.; Roselyn, J.P. Multimode Inverter Control Strategy for LVRT and HVRT Capability Enhancement in Grid Connected Solar PV System. *IEEE Access* **2022**, *10*, 54899–54911. [CrossRef]
9. Lin, X.; Han, Y.; Yang, P.; Wang, C.; Xiong, J. Low-Voltage Ride-Through Techniques for Two-Stage Photovoltaic System under Unbalanced Grid Voltage Sag Conditions. In Proceedings of the IEEE 4th Southern Power Electronics Conference (SPEC), Singapore, 10–13 December 2018; pp. 1–8.

10. Sabir, A. A novel low-voltage ride-through capable energy management scheme for a grid-connected hybrid photovoltaic-fuel cell power source. *Int. Trans. Electr. Energy Syst.* **2019**, *29*, e2713. [CrossRef]
11. Al-Shetwi, A.Q.; Sujod, M.Z. Modeling and control of grid-connected photovoltaic power plant with fault ride-through capability. *J. Sol. Energy Eng.* **2018**, *140*, 021001. [CrossRef]
12. Priya, R.P.; Mohanraj, M. Power quality improvement in grid connected wind energy system using fuzzy controlled UPQC. *Pak. J. Biotechnol.* **2017**, *14*, 17–20.
13. Park, S.M.; Park, S.Y. Power weakening control of the photovoltaic-battery system for seamless energy transfer in microgrids. In Proceedings of the IEEE Applied Power Electronics Conference and Exposition (APEC), Long Beach, CA, USA, 17–21 March 2013; pp. 2971–2976.
14. Kim, D.; Ramadhan, U.F.; Islam, S.U.; Jung, S.; Yoon, M. Design and implementation of novel fault ride through circuitry and control for grid-connected PV system. *Sustainability* **2022**, *14*, 9736. [CrossRef]
15. Nezhad, A.A.; Zaker, B.; Arani, A.A.K.; Gharehpetian, G.B. Impact of non-MPPT operation mode of PV system considering inverter fault current limiting. In Proceedings of the Conference on Electrical Power Distribution Networks Conference (EPDC), Semnan, Iran, 19–20 April 2017; pp. 45–50.
16. Almeida, P.M.; Monteiro, K.M.; Barbosa, P.G.; Duarte, J.L.; Ribeiro, P.F. Improvement of PV grid-tied inverters operation under asymmetrical fault conditions. *Sol. Energy* **2016**, *133*, 363–371. [CrossRef]
17. Bak, Y.; Lee, J.S.; Lee, K.B. Low-voltage ride-through control strategy for a grid-connected energy storage system. *Appl. Sci.* **2018**, *8*, 57. [CrossRef]
18. Lin, F.J.; Lu, K.C.; Ke, T.H.; Yang, B.H.; Chang, Y.R. Reactive power control of three-phase grid-connected PV system during grid faults using Takagi–Sugeno–Kang probabilistic fuzzy neural network control. *IEEE Trans. Ind. Electron.* **2015**, *62*, 5516–5528. [CrossRef]
19. Bagchi, S.; Chatterjee, D.; Bhaduri, R.; Biswas, P.K. An improved low-voltage ride-through (LVRT) strategy for PV-based grid connected inverter using instantaneous power theory. *IET Gener. Transm. Distrib.* **2021**, *15*, 883–893. [CrossRef]
20. Jinpeng, W.; Bo, Z.; Qinxue, Y.; Xin, Z. Research on the Automatically Independent Controlling Algorithm of the Grid-Connected PV Inverter Jointly Considering Dynamic Load Features and Active LVRT Capability. *IEEE Access* **2023**, *11*, 36618–36629. [CrossRef]
21. Hong, C.M.; Ou, T.C.; Lu, K.H. Development of intelligent MPPT (maximum power point tracking) control for a grid-connected hybrid power generation system. *Energy* **2013**, *50*, 270–279. [CrossRef]
22. Ou, T.C.; Hong, C.M. Dynamic operation and control of microgrid hybrid power systems. *Energy* **2014**, *66*, 314–323. [CrossRef]
23. Joshi, J.; Jately, V.; Kala, P.; Sharma, A.; Lim, W.H.; Azzopardi, B. Control strategy for current limitation and maximum capacity utilization of grid connected PV inverter under unbalanced grid conditions. *Sci. Rep.* **2024**, *14*, 10118. [CrossRef]
24. Zhang, N.; Sun, Q.; Yang, L.; Li, Y. Event-Triggered Distributed Hybrid Control Scheme for the Integrated Energy System. *IEEE Trans. Ind. Inform.* **2021**, *18*, 835–846. [CrossRef]
25. Saxena, V.; Kumar, N.; Singh, B.; Panigrahi, B.K. An MPC based algorithm for a multipurpose grid integrated solar PV system with enhanced power quality and PCC voltage assist. *IEEE Trans. Energy Convers.* **2021**, *36*, 1469–1478. [CrossRef]
26. Elmi, M.M.B.; Yıldırım, O. Improve LVRT capability of organic solar arrays by using chaos-based NMPC. *Int. J. Energy Stud.* **2024**, *9*, 543–558. [CrossRef]
27. Gira, N.; Dahiya, A.K. ANFIS controlled reactive power compensation utilizing grid-connected solar photovoltaic system as PV-STATCOM. *J. Sci. Ind. Res.* **2021**, *80*, 668–674. [CrossRef]
28. Li, X.; Chen, Y.; Yu, W.; Li, L.; Yao, P.; Lan, J.; Ai, J.; Chen, W. Virtual Inductance and DC Boosting Control Based Low Voltage Ride-Through Method for Doubly-Fed Variable-Speed Pumped Hydro Storage Units. *IEEE Trans. Power Electron.* **2026**, *41*, 6125–6135. [CrossRef]
29. Bangladesh Power Development Board. *Grid Code of Bangladesh*; Bangladesh Power Development Board: Dhaka, Bangladesh, 2019; Rep. GC-2019.
30. Ahmad, S.; Mekhilef, S.; Mokhlis, H. An intelligent interconnection module for multiple self-healed interconnected microgrids. In Proceedings of the IEEE 4th International Conference on Computing, Power and Communication Technologies (GUCON), Kuala Lumpur, Malaysia, 24–26 September 2021; pp. 1–6.
31. Tasnim, M.N.; Ahmed, T.; Dorothi, M.A.; Ahmad, S.; Shafiullah, G.M.; Ferdous, S.M.; Mekhilef, S. Voltage-oriented control-based three-phase, three-leg bidirectional AC–DC converter with improved power quality for microgrids. *Energies* **2023**, *16*, 6188. [CrossRef]
32. Tasnim, M.N.; Ahmed, T.; Dorothi, M.A.; Ahmad, S.; Shafiullah, G.M.; Ferdous, S.M.; Mekhilef, S. Autonomous power management and control among interconnected standalone hybrid microgrids. In Proceedings of the IEEE International Conference on Power Systems (ICPS), Cox's Bazar, Bangladesh, 13–15 December 2023; pp. 1–6.
33. Al-Shetwi, A.Q.; Sujod, M.Z.; Blaabjerg, F. Low voltage ride-through capability control for single-stage inverter-based grid-connected photovoltaic power plant. *Sol. Energy* **2018**, *159*, 665–681. [CrossRef]

34. Ahmad, S.; Jhuma, U.K.; Karimi, M.; Pourdaryaei, A.; Mekhilef, S.; Mokhlis, H.; Kauhaniemi, K. Direct power control based on point of common coupling voltage modulation for grid-tied AC microgrid PV inverter. *IEEE Access* **2022**, *10*, 109187–109202. [CrossRef]
35. Ahmad, S.; Mekhilef, S.; Mokhlis, H.; Karimi, M.; Pourdaryaei, A.; Ahmed, T.; Jhuma, U.K.; Afzal, S. Fuzzy logic-based direct power control method for pv inverter of grid-tied ac microgrid without phase-locked loop. *Electronics* **2021**, *10*, 3095. [CrossRef]
36. Ding, G.; Gao, F.; Tian, H.; Ma, C.; Chen, M.; He, G.; Liu, Y. Adaptive DC-link voltage control of two-stage photovoltaic inverter during low voltage ride-through operation. *IEEE Trans. Power Electron.* **2015**, *31*, 4182–4194. [CrossRef]
37. Mahmud, S.I.; Mannan, M.A.; Hazari, M.R. Design and Performance Analysis of a PV Control Scheme to Improve LVRT of Hybrid Power System. *AIUB J. Sci. Eng.* **2021**, *20*, 20–21. [CrossRef]
38. Wen, H.; Fazeli, M. A low-voltage ride-through strategy using mixed potential function for three-phase grid-connected PV systems. *Electr. Power Syst. Res.* **2019**, *173*, 271–280. [CrossRef]
39. Al-Shetwi, A.Q.; Sujod, M.Z.; Ramli, N.L. A review of the fault ride through requirements in different grid codes concerning penetration of PV system to the electric power network. *ARPN J. Eng. Appl. Sci.* **2015**, *10*, 9906–9912.
40. Ahmad, S.; Mekhilef, S.; Mokhlis, H. DQ-axis synchronous reference frame-based PQ control of grid connected AC microgrid. In Proceedings of the IEEE International Conference on Computing, Power and Communication Technologies (GUCON), Greater Noida, India, 2–4 October 2020; pp. 842–847.
41. Hannan, M.A.; Ghani, Z.A.; Hoque, M.M.; Ker, P.J.; Hussain, A.; Mohamed, A. Fuzzy logic inverter controller in photovoltaic applications: Issues and recommendations. *IEEE Access* **2019**, *7*, 24934–24955. [CrossRef]
42. Orłowska-Kowalska, T.; Blaabjerg, F.; Rodríguez, J. (Eds.) *Advanced and Intelligent Control in Power Electronics and Drives*; Springer: Berlin/Heidelberg, Germany, 2014.
43. Roselyn, J.P.; Chandran, C.P.; Nithya, C.; Devaraj, D.; Venkatesan, R.; Gopal, V.; Madhura, S. Design and implementation of fuzzy logic based modified real-reactive power control of inverter for low voltage ride through enhancement in grid connected solar PV system. *Control Eng. Pract.* **2020**, *101*, 104494. [CrossRef]